JACS
JOURNAL OF THE AMERICAN CHEMICAL SOCIETY
Article
pubs.acs.org/JACS

Large-Scale Screening of Zeolite Structures for CO_2 Membrane Separations

Jihan Kim,*[,†] Mahmoud Abouelnasr,[‡] Li-Chiang Lin,[‡] and Berend Smit[†,‡,§]

[†]Materials Sciences Division, Lawrence Berkeley National Laboratory, Berkeley, California 94720, United States
[‡]Department of Chemical and Biomolecular Engineering and [§]Department of Chemistry, University of California, Berkeley, California 94720, United States

Supporting Information

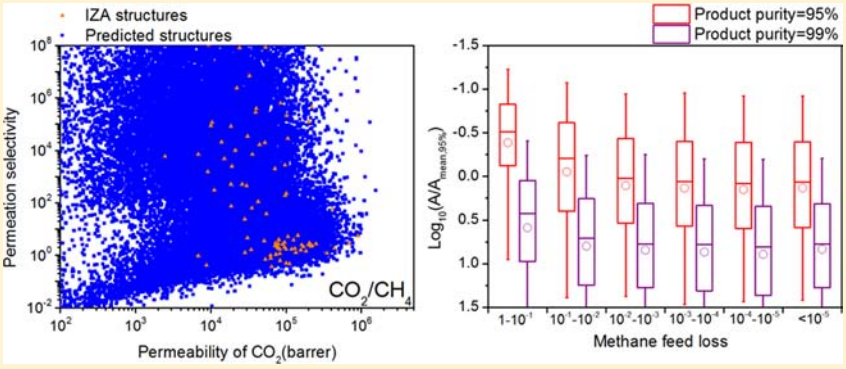

ABSTRACT: We have conducted large-scale screening of zeolite materials for CO_2/CH_4 and CO_2/N_2 membrane separation applications using the free energy landscape of the guest molecules inside these porous materials. We show how advanced molecular simulations can be integrated with the design of a simple separation process to arrive at a metric to rank performance of over 87 000 different zeolite structures, including the known IZA zeolite structures. Our novel, efficient algorithm using graphics processing units can accurately characterize both the adsorption and diffusion properties of a given structure in just a few seconds and accordingly find a set of optimal structures for different desired purity of separated gases from a large database of porous materials in reasonable wall time. Our analysis reveals that the optimal structures for separations usually consist of channels with adsorption sites spread relatively uniformly across the entire channel such that they feature well-balanced CO_2 adsorption and diffusion properties. Our screening also shows that the top structures in the predicted zeolite database outperform the best known zeolite by a factor of 4−7. Finally, we have identified a completely different optimal set of zeolite structures that are suitable for an inverse process, in which the CO_2 is retained while CH_4 or N_2 is passed through a membrane.

INTRODUCTION

Elevated CO_2 concentrations in the atmosphere are considered to be the primary cause of global warming.[1] Because of the ever-increasing amount of CO_2 emissions and our continuing reliance on fossil fuels, it remains imperative to search for various methods to mitigate the emission process. Among many suggested solutions, carbon capture and sequestration (CCS) is emerging as a viable technique:[2] CCS consists of utilizing materials to capture CO_2 emissions from point sources such as electric power plants, cement and steel plants, or natural gas field and injecting the adsorbed CO_2 molecules to geological reservoirs. Some of the main barriers for the large-scale implementation of CCS are the energy requirements and cost of the capture process.

The currently available technology uses amines to selectively absorb CO_2. These amines are very efficient in absorption of CO_2, but the regeneration of the amine solution is relatively energy intensive. Alternative technologies, such as adsorption by adsorbents[3] or separations using membranes,[4] have the potential to significantly reduce the energy costs. Both technologies depend on the development of novel materials that have optimal properties for a given separation, with important classes of materials being nanoporous solids, such as zeolites and metal−organic frameworks.[3,5−8] By changing the pore topology and chemical composition, one could, in principle, synthesize millions of different materials, making it difficult to experimentally characterize and test all these materials. This gives a great opportunity for molecular simulations to identify the optimal materials *in silico* and guide the direction of the experimental research.

To this end, we present a novel computational approach that lets us efficiently predict the permeation of a material for membrane separation appications. Recently, there have been several articles that pertain to computational screening of a large database of porous materials in search for optimal

Received: January 9, 2013
Published: April 25, 2013

   dx.doi.org/10.1021/ja400267g | *J. Am. Chem. Soc.* 2013, 135, 7545−7552

materials for CCS.[3,9−14] However, most of these calculations focus on adsorption processes; in contrast, far less attention has been given to screening for membrane processes.[15,16] The main reason for this is that the screening of membranes requires, in addition to the adsorption properties, also information about the diffusion coefficients. However, most diffusion coefficient calculations require expensive molecular dynamics (MD) simulations, and as such, much work in the past has focused on analyzing only 10−20 structures.[9] To avoid conducting MD simulations for thousands of structures, one can apply a geometric criterion to select those materials for which one component can enter but not the other.[16−18] This is a very efficient method to screen materials with very high diffusive selectivity, but not necessarily for high permeability. Moreover, the geometric approach ignores the energy interactions between the guest particle and the host framework atoms, which leads to predicted diffusion properties that are independent of the specific chemistry used to functionalize a material. In this work, we demonstrate that a reliable estimate of the diffusion coefficient can be obtained from a free energy calculation. In this approach, we take full advantage of the information contained within the free energy landscape throughout the entire unit cell of the crystal structure and apply the transition-state theory (TST) to calculate the diffusion properties.[19,20] Mapping this algorithm to the high-throughput processing power of the graphics processing units (GPUs), we have accurately characterized the adsorption and the diffusion properties of over 87 000 experimental International Zeolite Association (IZA) structures and predicted pure-silica zeolite structures from Deem's database.[21,22] For the predicted zeolite database, PCOD (Predicted Crystallography Open Database), a set of 330 000 structures within +30 kJ/mol Si of α-quartz was further reduced to 139 397 by removing structures with largest free-sphere diameter below 3.25 Å.[23] From the reduced set, we selected over 87 000 zeolite structures that have orthogonal unit cells to facilitate calculations. Similar work has been conducted by Haldoupis et al., but their approach was limited to computing diffusion coefficients of spherical molecules such as CH_4.[24] Our method can compute diffusion coefficients of both spherical and nonspherical molecules within a single structure in just a few seconds, providing the speed-up required to screen thousands of different structures. Moreover, our algorithm explores the entire channel profile and identifies multiple channels and free-energy barrier locations, which can provide a more accurate picture of diffusion in porous materials. At this point, it is important to note that zeolitic membranes have been synthesized.[25,26] However, these studies have been limited to a few pore topologies, so an important practical question we would like to address is whether these materials are close to the optimal performance, or whether significant gains can be expected if one would try to synthesize a membrane using a different zeolite topology.

To illustrate how our screening can be used to find the optimal material, we use as an example the separation of CO_2 from CH_4 in natural gas reservoirs. Natural gas reservoirs may contain up to 70% CO_2, and the production of these reservoirs would require the separation of CO_2 from the natural gas and injection back into the reservoir. As CH_4/CO_2 has high pressure, membranes are ideal to carry out this separation efficiently. At this point, it is important to emphasize that the ideal material for a separation depends on the actual process requirements. We use our screening approach to illustrate this point with a simple model that mimics the separation of CH_4 from CO_2 at conditions typical of a natural gas reservoir. The increase in efficiency of our method allows us to screen many materials and identify the optimal structures for an entire class of materials. Establishing such a theoretical limit provides important guidance for future material synthesis. Our study identifies the general characteristics of the best-performing structures. It can be expected that, in other classes of materials, structures with similar characteristics will also perform very well.

RESULTS AND DISCUSSION

The transport of molecules through a membrane can be characterized by its permeability. The permeability is defined as the product of the solubility and the diffusion coefficient of the gas molecules. As such, permeability is a crucial component for evaluating membrane performance,[4] and it requires computation of both adsorption and diffusion properties of the system. For the adsorption part, we use existing computational methods based on GPUs.[12] The methodology used to compute the diffusion coefficients described in the Methods section has been implemented for this work. We have selected a set of representative experimental zeolite structures from the IZA database to test our method. Figure 1 compares the self-diffusion coefficient (D_S) of CO_2, N_2, and CH_4 gas molecules at infinite dilution and T = 300 K for the two methods, and it shows that our method provides a reasonably accurate description of the diffusion. The discrepancies between the two methods result from a variety of different reasons such as correlated hops for large diffusion values[19] and the presence of complicated channel profiles that makes very accurate TST analysis difficult. In general, the MD simulation wall time scales with the inverse of D_S, becoming intractable in slowly diffusing systems as hops across a large barrier becomes increasingly rare. Accordingly, given that our model based on the TST uses an algorithm where the wall time remains independent of the diffusive coefficient values, an enormous speed-up (few seconds versus several weeks) can be gained compared to MD simulations in structures with small D_S.

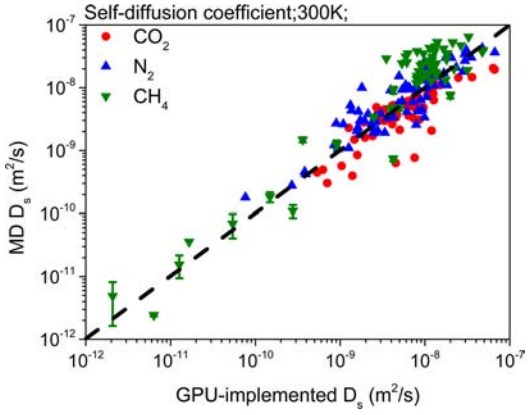

Figure 1. Comparison of two different methods (MD and GPU-implemented TST) to compute the self-diffusion coefficients of CO_2 (red circles), N_2 (blue up-triangles), and CH_4 (green down-triangles) molecules for IZA zeolite structures. The dashed line indicates the region of perfect agreement between the two methods. The error bars from the MD simulations are provided for only a few selected zeolite structures.

dx.doi.org/10.1021/ja400267g | J. Am. Chem. Soc. 2013, 135, 7545−7552

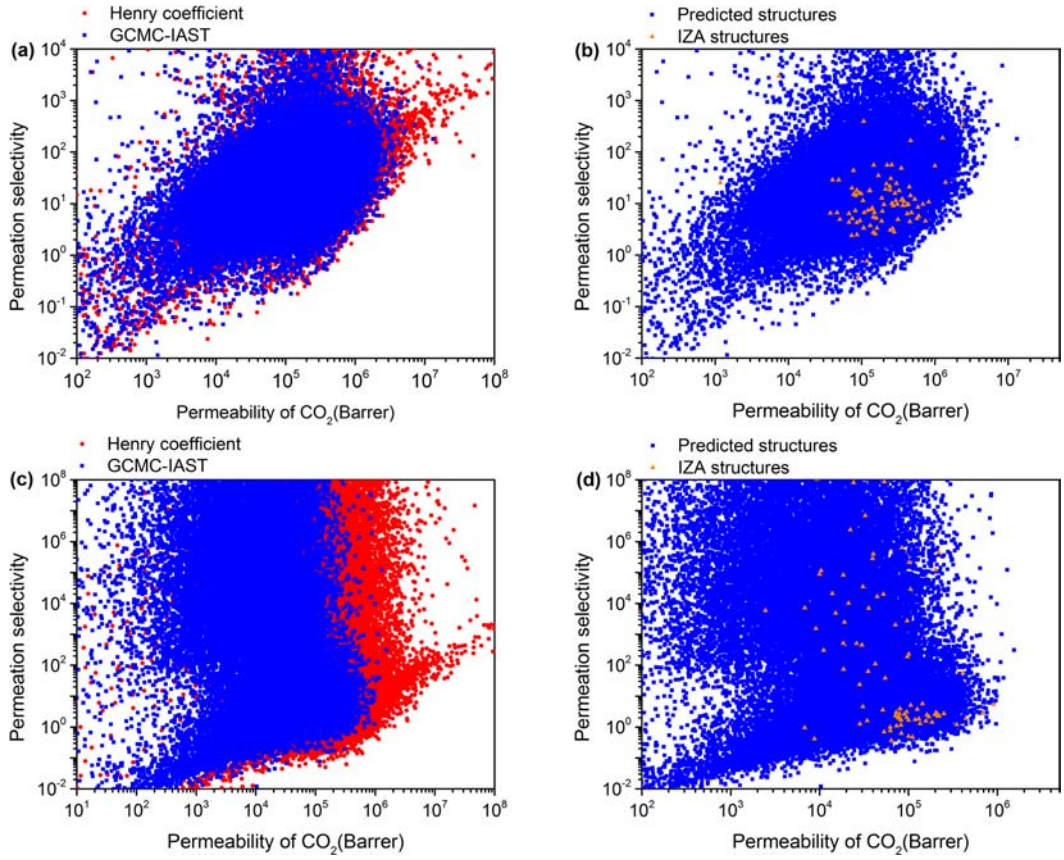

Figure 2. Permeation selectivity as a function of CO_2 permeability for (a) CO_2/N_2 separations (K_H, red; GCMC-IAST, blue), (b) CO_2/N_2 separations for GCMC-IAST in predicted (blue) and IZA (orange) zeolites, (c) CO_2/CH_4 separations (K_H, red; GCMC-IAST, blue), and (d) CO_2/CH_4 separations for GCMC-IAST in predicted (blue) and IZA (orange) zeolites.

Figure 1 also illustrates that the zeolite data points for CO_2 and N_2 are concentrated in the highly diffusive region (i.e., $D_S > 10^{-9}$ m^2/s), whereas CH_4 data points are scattered across a wider range of D_S values. Because the kinetic diameter of CH_4 is larger than both CO_2 and N_2, there exists more structures with relatively smaller diffusion coefficients for CH_4. Also, due to the long-range electrostatic interactions present for the nonpolar CO_2 and N_2 molecules with quadruple moments, the likelihood of finding structures with a relatively high energy barrier remains small as the contributions of the nonlocal interactions spread across the entire channel. On the other hand, the lack of electrostatic interactions in CH_4 molecules translates into free energy landscapes that are determined solely by short-range interactions from the neighboring framework atoms, which enhances the likelihood of finding channels with a narrow, pinched region (i.e., large energy barrier) separating the adsorption sites for certain topologies.

Next, we explore the different characteristics between CO_2/CH_4 and CO_2/N_2 separations for the zeolite structures. For analysis, we included over 87 000 predicted zeolite structures in order to detect possible patterns that can emerge for the entire class of materials and for selected separations that might not be obvious in analyzing just a few structures. In most membrane research, the relative performance of a material is estimated from a Robeson plot, which gives the relationship between permeability and the permeation selectivity.[27] In all cases, the permeation selectivity value less than one indicates that the membrane is selective but the CO_2 ends up in the retentate. Figure 2a,b shows the zeolite Robeson plots for CO_2/N_2, and Figure 2c,d shows those for CO_2/CH_4 separations. We considered two different methods to compute the adsorption component of the permeability and permeation selectivity: (1) using the Henry coefficient, K_H, which gives an accurate description of the adsorption at low pressures and (2) using the grand canonical Monte Carlo (GCMC) simulations for obtaining pure component isotherm and applying the ideal adsorbed solution theory (IAST) for estimating mixture adsorption at given condition.[28] In general, using K_H values overestimates the permeability, as shown in the Robeson plots in Figure 2a,c (red data points). Since most gas separation occurs at higher pressures, the uptake values at the actual separation pressure provides a better measure of permeability compared to K_H. For CO_2/N_2 separations the flue gas operating condition of total fugacity equal to 1 bar (14% CO_2 and 86% N_2) was used, while for CO_2/CH_4 the total fugacity of 10 bar (50% CO_2 and 50% CH_4) was used. Upon increasing the pressure, the gas uptake begins to saturate; thus, the adjusted permeability value based upon GCMC-IAST becomes smaller at pressures outside of the linear Henry regime. Because CO_2/N_2 separation occurs at a lower pressure compared to CO_2/CH_4 separation, the overall shift in the data points in the Robeson plots (indicating decrease in CO_2 permeability) in Figure 2c becomes more apparent for CO_2/CH_4.

It is instructive to compare our results with the well-known Robeson plots for polymer materials. For these materials, one typically observes a limiting behavior, the Robeson upper bound, as materials that have high selectivity have low

dx.doi.org/10.1021/ja400267g | J. Am. Chem. Soc. 2013, 135, 7545−7552

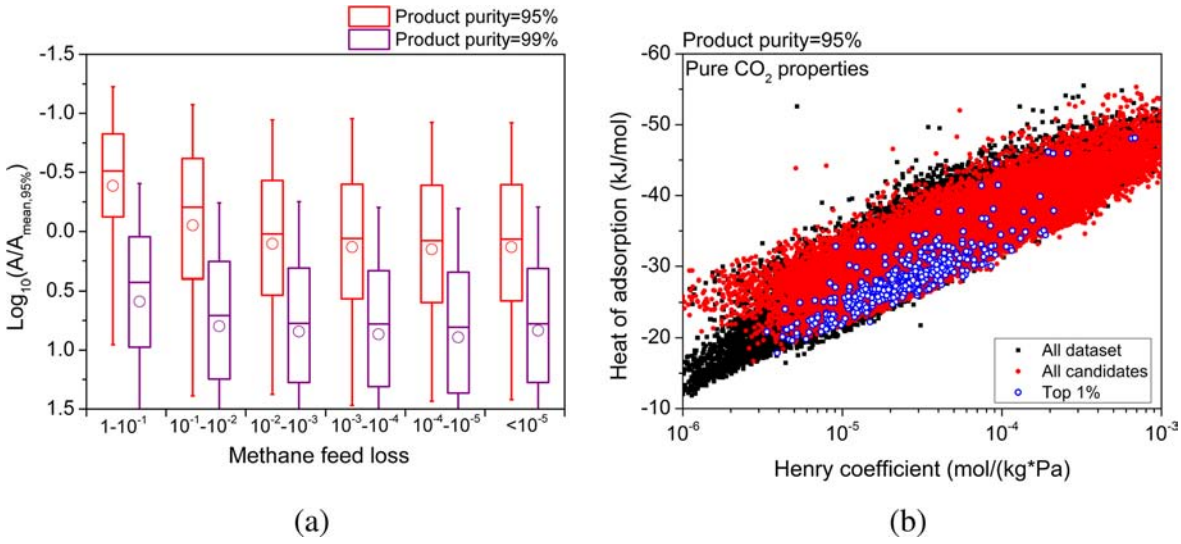

Figure 3. (a) Membrane area as a function of CH_4 feed loss for zeolite structures that satisfy the minimum purity requirement of 95% (red) and 99% (purple). $A_{mean,95\%}$ is defined as the logarithm averaged area with the given 95% purity. The segments within each box from bottom to top represent the 5%, 25%, 50%, 75%, and 95% points for each bin with the circle indicating the average value for the whole bin. (b) Heat of adsorption as a function of CO_2 K_H for all zeolite data sets (black), selected candidate sets that satisfy the 95% purity requirement (red), and the top 1% best-performing structures from the set of all candidate structures (blue).

permeability and materials with high permeability have low selectivity.[27,29] In the literature, deviations from this Robeson upper bound have been reported for nanoporous materials.[30] Figure 2 shows, however, that nanoporous materials have a qualitatively very different behavior, in which the concept of a Robeson upper limit has little value. The reason is that the difference in solubility of guest molecules in these materials can vary orders of magnitudes, while in the Robeson upper limit, it is assumed that all materials have a similar solubility.[29]

In Figure 2, most of the data points in the CO_2/N_2 Robeson plot are concentrated in a narrow band of permeation selectivity values and indicates a general positive correlation between CO_2 permeability and CO_2/N_2 permeation selectivity. On the other hand, the data points for the CO_2/CH_4 Robeson plots are spread across a wider range of selectivity values with less meaningful correlations being found between permeability and selectivity. Because both CO_2 and N_2 molecules are non-polar with quadruple moments, linear, and have comparable kinetic diameters, the diffusion properties of the two gas molecules are similar. Moreover, the values of $K_H^{N_2}$ of the entire database are in a much narrower range compared to the corresponding values of $K_H^{CO_2}$. Accordingly, given this narrow range of $K_H^{N_2}$ values and similar diffusive properties between CO_2 and N_2, the shape of the Robeson plot is dictated largely by $K_H^{CO_2}$, which is positively correlated in both the permeability and the permeation selectivity. The CO_2/N_2 points located along a narrow band can be also seen in the CO_2/CH_4 Robeson plot as well. However, additional, more scattered data points exists in this Robeson plot, which is caused by the dissimilarity between the CO_2 and the CH_4 molecules. Most of these outliers correspond to zeolite structures that possess very narrow channels, leading to relatively low CH_4 diffusion coefficient values or from different CO_2/CH_4 adsorption sites.

To identify the structures most promising for CO_2/N_2 and CO_2/CH_4 separations, a suitable metric that can quantify the material performance needs to be constructed. A diagram that illustrates the CO_2/CH_4 separation process is shown in Figure SI1 (Supporting Information). The target for the CO_2/CH_4 separation is to obtain a high purity CH_4 stream in the retentate side. The conventional approach in identifying the top performing structures for such a membrane separation is to select those materials that have the highest permeability and selectivity. We use a simple membrane design to illustrate that from a practical point of view, this criterion does not provide us the optimal material. The argument that one needs to be in the upper right corner in the Robeson plot (i.e., high permeability and selectivity region) assumes that selectivity is equally important as permeability. Our analysis shows that for a given separation, one needs a minimum selectivity; the best material is the one with highest permeability out of all materials that satisfy this minimum selectivity criterion. Selectivity is the dominant factor only for separations that require an extremely high purity. Baker et al. reached a similar conclusion for the N_2/CO_2 separation.[4] In an ideal membrane system, the area of the membrane is assumed to be a measurement of the cost of the entire process, and this area is shown to be mainly dominated by and inversely proportional to the CO_2 permeability (for more detailed derivation, see Supporting Information, Section 2). Hence, we can rank those materials that satisfy the minimum selectivity criterion based on the membrane area that is required for the separation.

With a working performance metric at hand, we plot the membrane area as a function of CH_4 feed loss (i.e., 1 − methane recovery) for materials that satisfy the methane purity criteria of 95% and 99% purities in Figure 3a. The feed loss gives us the amount of methane that we inject with the CO_2 in the reservoir. As we are screening many materials, a clear trend emerges with some structures that have nearly ideal properties and have therefore, an exceptionally high performance. However, from a synthetic point of view, it might be very difficult to synthesize exactly these materials. In Figure 3a, the box representation is used to indicate the exceptional materials and show the general trend: the lines above and below the boxes show the structures with good and poor performance, and the boxes show the trends as represented by a large number of structures that have the same properties. In the

dx.doi.org/10.1021/ja400267g | J. Am. Chem. Soc. 2013, 135, 7545−7552

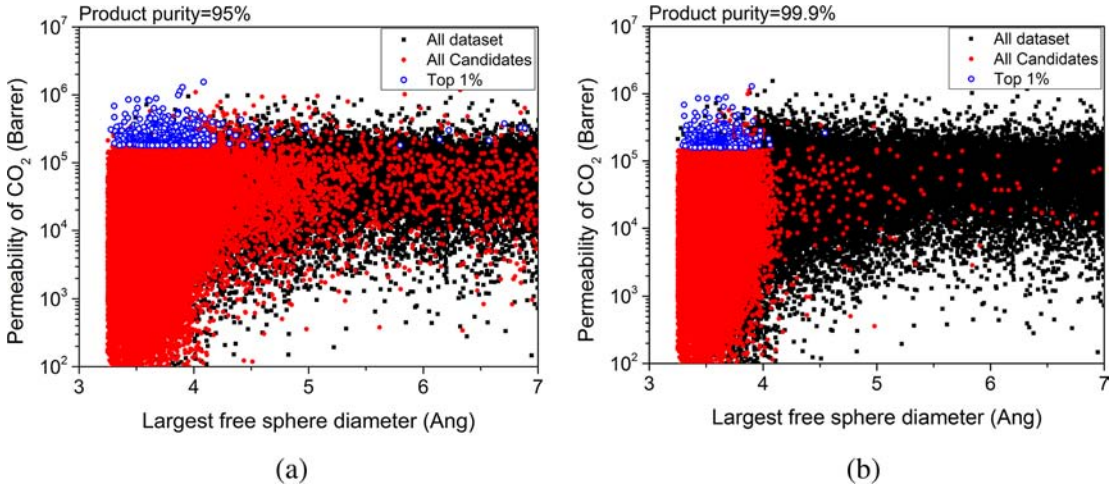

Figure 4. CO_2 permeability as a function of largest free sphere diameter for (a) 95% CH_4 purity and (b) 99.9% CH_4 purity for all the zeolites in the data set (solid black), the candidate subsets that fulfill the purity requirement (solid red), and the top 1% structures (i.e., top 1% in area with recovery >90%) (open blue).

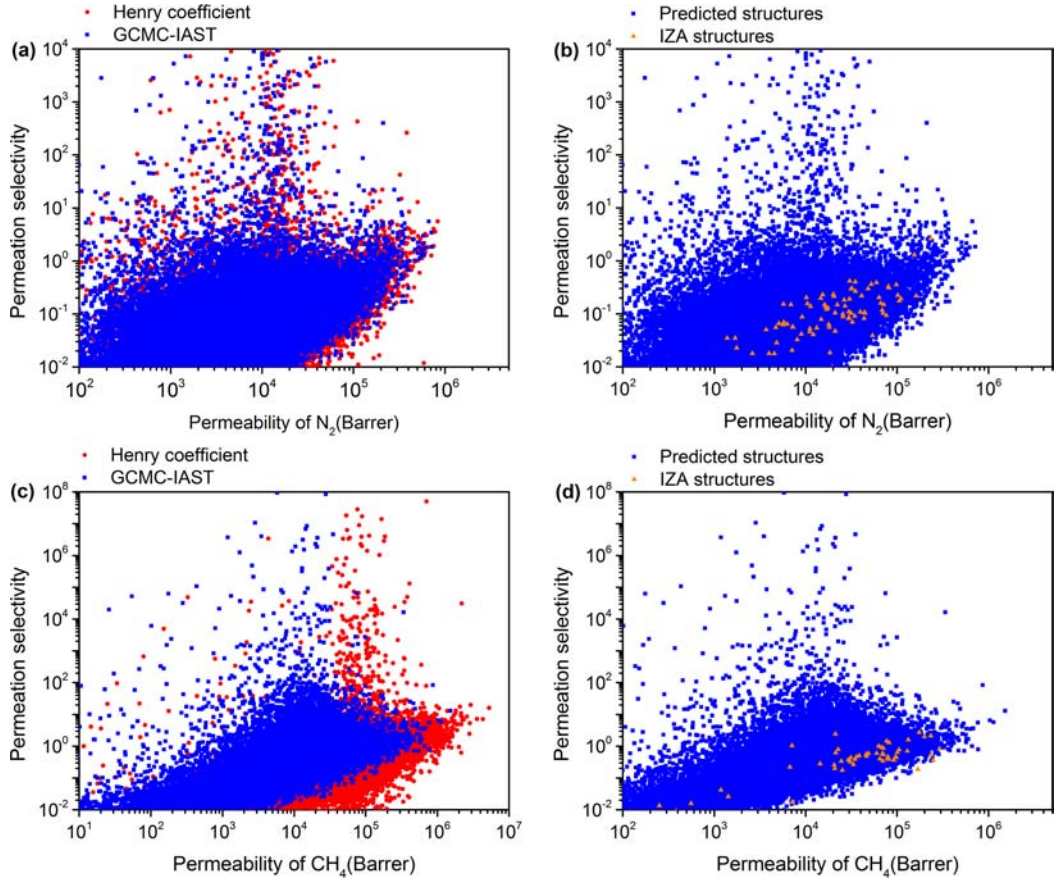

Figure 5. Permeation selectivity as a function of N_2 permeability for (a) CO_2/N_2 inverse separations (K_H, red; GCMC-IAST, blue) and (b) CO_2/N_2 inverse separations for GCMC-IAST in predicted (blue) and IZA (orange) zeolites. Permeation selectivity as a function of CH_4 permeability for (c) CO_2/CH_4 inverse separations (K_H, red; GCMC-IAST, blue) and (d) CO_2/CH_4 inverse separations for GCMC-IAST in predicted (blue) and IZA (orange) zeolites.

following, we focus on these general trends. As expected, the membrane area tends to increase for smaller membrane feed loss, indicating that if we require a higher selectivity, we will have less materials to choose from.

For a specified purity requirement, we can isolate the top structures and identify common features that separate these structures from the others. For example, we plot the CO_2 heat of adsorption as a function of the Henry coefficient, $K_H^{CO_2}$, for the top 1% structures that satisfy the product purity requirement of 95%. The best structures possess Henry coefficient that is in the intermediate range ($10^{-5} < K_H^{CO_2} < 10^{-4}$ mol/(kg·Pa)). In structures that have very small $K_H^{CO_2}$, the overall CO_2 permeability and the permeation selectivity is too small, making them suboptimal for membrane separations.

dx.doi.org/10.1021/ja400267g | J. Am. Chem. Soc. 2013, 135, 7545−7552

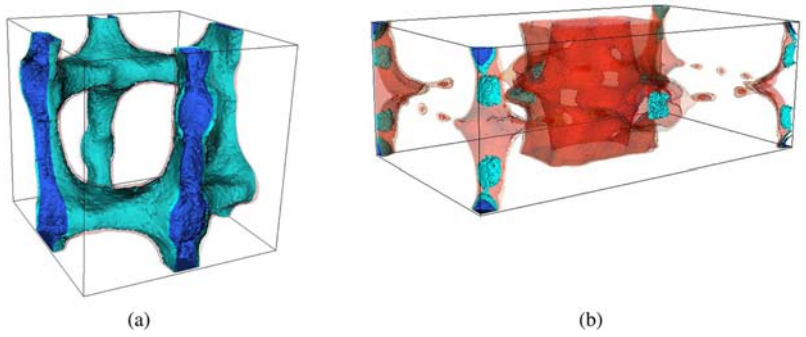

Figure 6. (a) CO_2 free energy landscape within a unit cell of GIS structure, which is predicted to be one of the best structures for both CO_2/N_2 and CO_2/CH_4 separations. (b) CO_2 free energy landscape within a unit cell of PCOD8198030 structure, which is predicted to be one of the best structures for CH_4/CO_2 inverse separation. The blue regions indicate low-energy adsorption sites (minima values of −4493 and −6775 K for GIS and PCOD8198030, respectively), the red indicates relatively high energy regions while the rest represents inaccessible regions.

In structures that have too large of $K_H^{CO_2}$ ($K_H^{CO_2} > 10^{-3}$ mol/(kg·Pa)), one key factor comes into play that degrade performance: there is an inverse relationship between $K_H^{CO_2}$ and D_S, as can be seen from Figure SI3. Structures with large $K_H^{CO_2}$ possess strong adsorption sites that cause the diffusion rate to decrease as the effective barrier separating one adsorption site to another becomes large. Among structures that are inside the optimal Henry coefficient range, the optimal structures tend to have low heat of adsorption values (blue data points in Figure 3b). A high heat of adsorption often corresponds to strong adsorption sites, which lead to low diffusion coefficients.

At this point, it is instructive to compare our results with those from geometrical screening.[16] Geometrical screening identifies the best materials as the ones that possess pore diameter values similar to the kinetic diameter of the molecules that have to be separated. Intuitively, this makes sense as one can imagine that the separation process will be optimized when one guest molecule species is just small enough to diffuse across the channel, while the larger one being blocked. To gain insights in the differences between the two methods, we plot the CO_2 permeability as a function of the largest free sphere diameter (D_f)[23] for all structures shown in Figure 4. The largest free sphere diameter is a measure of the size of the molecule that can enter a particular structure. A simple geometric criterion is to select those structures that have a D_f large enough for CO_2 to enter but too small for CH_4. In our analysis, two important points emerge that cannot be deduced from a pure geometrical analysis. First, few high performing structures possess very large D_f values, which deviates from what is predicted from geometrical analysis. Because most geometrical analysis focuses on selectivities, only the structures that consists of pore diameters that are close to the size of the guest molecules are deemed interesting and worthwhile for investigation. Our energy-based method reveals that for 95% purity requirement, one can identify structures that lie outside of this region (blue data points for $D_f > 4$ Å in Figure 4a). Once the desired purity is set to be very large at 99.9% (Figure 4b), the best-performing structures tend to be concentrated in the region $D_f = 3-4$ Å. For such a high purity, it is essential to have high selectivity and the geometric criterion ensures this. The second important point is that our method can readily differentiate large and small CO_2 permeability values in structures that are located within the optimal D_f values (3−4 Å) as our method can compute accurate D_S values. Accordingly, the set of potential candidates for membrane separation can be further refined using the energy-based analysis.

Until now, we have assumed that CO_2 is the component with the highest permeation. As this is the case for most known porous materials, one normally does not consider a separation where CH_4 or N_2 is assumed to be the component with the highest permeability. Such a material, however, would be of interest as it would allow for separation in which the CO_2 is retained while preferring permeability of CH_4 or N_2. This process can be attractive since in the conventional process, the CO_2-rich stream is the low-pressure permeate and hence needs to be repressurized for transportation and storage, while in the inverse process, the CO_2-rich stream is the retentate and repressurizing is not required. Such process will be particularly attractive for those natural gas fields in which the CO_2 concentration exceeds 50%. Figure 5 shows the Robeson plots corresponding to this separation where the same data points from Figure 2 were plotted with inverted permeation selectivity values. In general, the permeability as well as the selectivity for the top performing structures are predicted to be lower as the number of structures that possess larger CH_4 and N_2 uptake values compared to the CO_2 uptake values at the interested separation process is very small. We did not identify any of the known experimental (IZA) zeolite structures that possessed CH_4/CO_2 or N_2/CO_2 permeation selectivity values >10. On the other hand, screening of the predicted zeolite structures does reveal a large number of structures that would allow for such a separation, suggesting such a separation is possible.

It is interesting to make comparisons between the best predicted zeolite structure and the best IZA structure we identified from our screening analysis. In our evaluation, the membrane area, which is dominated by and inversely proportional to the CO_2 permeability is used as a metric that needs to be minimized to have the best membrane separation performance. The ratio between the smallest membrane area found in the IZA and the PCOD structures are defined as the performance gain.[22] For CO_2/CH_4, this gain ranges from 4 to 7 for differing minimum selectivity requirements that range from 85 to 98% purity with the recovery set at 0.90. Among the IZA structures, ABW and GIS zeolite structures were identified to have the largest CO_2 permeability as both of these structures possess relatively strong CO_2 adsorption sites spread throughout the entire main channels. The $K_H^{CO_2}$ values computed at $T = 300$ K are 5.42×10^{-5} and 1.45×10^{-4} mol/(kg·Pa), while the D_S values are 8.01×10^{-9} and $3.51 \times$

dx.doi.org/10.1021/ja400267g | J. Am. Chem. Soc. 2013, 135, 7545−7552

10^{-9} m^2/s, respectively, for ABW and GIS. These values indicate that the best IZA structures do not possess exceptional adsorption or diffusive properties but are well-balanced in both. Figure 6a shows the CO_2 free energy landscape within the GIS structure where blue regions indicate relatively strong adsorption regions. The best PCOD structures for CO_2/CH_4 is identified to be PCOD8186909. Similar to ABW and GIS, the best predicted structures also show well-balanced adsorption and diffusion properties. Finally, for the structures optimal for the inverse process shown in Figure 5, the best structures tend to have strong CO_2 binding sites that reduce its diffusion coefficient to lower the CO_2 permeability. Concurrently, these structures possess strong enough CH_4 binding sites with fast enough diffusive properties for CH_4 to make them optimal for the inverse process. A sample structure (i.e., PCOD8198030) is shown in Figure 6b, where a significant energy barrier exists in the main channel for CO_2 molecules with the strongest adsorption sites.

CONCLUDING REMARKS

In summary, we have implemented an efficient method to determine diffusion coefficients based on the application of the transition state theory to the energy landscape of a large collection of structures. These diffusion properties, when combined with adsorption properties, can characterize the membrane performance for a given nanoporous material. Applying this method to a database of over 87 000 predicted zeolite structures, we found that for CO_2/CH_4 separations, the best-performing predicted structure can improve the performance as measured by the required area of a membrane by a factor of 4−7 compared to the best known zeolite structure.

Robeson plots for the CO_2/CH_4 separation reveal two distinct subclasses of structures: (1) a group with a relatively low permeation selectivity which varies in proportion to the permeability of CO_2, and (2) a group with much higher permeation selectivities which is presumed to arise mainly from diffusion selectivity, i.e., molecular sieving. These two different groups are not as clearly observed for the CO_2/N_2 separation, since the two particles have more similar dimensions, making molecular sieving less possible. The best material achieves a high selectivity without creating adsorption sites that slow down the diffusion. A simple experimental signature to recognize such a material for CO_2/CH_4 separation is a material that has intermediate range of CO_2 Henry coefficient (i.e., $10^{-5} < K_H^{CO_2} < 10^{-4}$ mol/(kg·Pa)) and a relatively low heat of adsorption (i.e., −30 to −20 kJ/mol).

METHODS

Although we focus mostly on zeolite structures with CO_2, N_2, and CH_4 as resident gas molecules, the techniques developed to compute the diffusion coefficients can readily extend to other gas molecules and to other materials. In our calculations, we assume that the zeolites are perfect, infinitely large crystals such that the periodic boundary conditions can be used. The number of unit cells is chosen such that the simulation box extends at least twice the cutoff radius of 12 Å in all three perpendicular directions. The host framework atoms are assumed to be rigid, and the pairwise gas−gas and gas−host interactions consist of Lennard-Jones forces and electrostatic interactions. The force fields developed by Garcia-Perez et al. are used in all of our work as they have been shown to be transferrable for variety of zeolite structures.[31] The temperature is set to be 300 K in all of the work. The MD simulations were conducted utilizing the CPU cores in our own cluster while the efficient diffusion coefficient calculations and the GCMC simulations were conducted utilizing the NVIDIA Tesla C2050 GPU cards from the Dirac Cluster at the National Energy Research Supercomputing Center (NERSC).

Molecular Dynamics Simulations. For an MD simulation, the gradient of the potential energy with respect to position is calculated for each adsorbate particle, including the van der Waals forces and Coulombic forces. This energy gradient manifests as a force which, constrained by intramolecular considerations, results in an acceleration according to Newton's second law of motion. In an MD simulation, the force on each particle is sampled periodically, allowing an update to each particle's position and velocity. With sufficiently small time steps (0.5 fs) and sufficiently long simulations (>1 ns), a collection of trajectories produced from MD simulations can be analyzed to calculate the self-diffusion coefficient.[32] In this study MD simulations were carried out in the canonical ensemble, using a Nosé−Hoover thermostat.

Efficient Diffusion Coefficient Calculations. At the start of the simulation, an energy grid that contains detailed information about the free energy profile of the gas molecules inside the porous material is constructed and subsequently analyzed to obtain both the adsorption and the diffusion properties of the system. A sufficiently fine mesh size of 0.1 Å is chosen for all structures and the resulting grid is superimposed on top of a single unit cell, where each of the grid points represents the total pairwise free-energy summation between the gas molecule and all of the framework atoms. For gas molecules such as CO_2 and N_2, which cannot be represented as a point particle, 250 randomized center-of-mass rotations of the molecule are conducted on the grid point to obtain an average Boltzmann-weighted free energy of the gas molecule at that point. The expression for free energy, F_i, at a specific grid point is expressed as follows:

$$F_i = -k_B T \log \frac{\sum_{j=0}^{N_{tot}} \exp\left(-E_j/k_B T\right)}{N_{tot}}$$

where N_{tot} = 250 and E_j is the potential energy of CO_2 (or N_2) molecule of a given randomized j configuration. For zeolite structures, the number of energy grid points is typically on the order of 10^6 and 10^7, and the calculations only take a few seconds using our GPU code.

From the constructed energy grid, points where $F_i < 15k_BT$ are considered accessible, while the rest are inaccessible. The choice of the $15k_BT$ cutoff was made such that energy values higher would be considered inaccessible during a typical experimental time scale.[12] The binary information (i.e., accessible/inaccessible) stored in a separate grid can be used to determine both the number of the channels and the channel direction. For example, in determining the number of channels along a given spatial direction (e.g., x direction), a two-dimensional flood fill algorithm at $x = 0$ along the y,z plane is used to combine the adjacent accessible points together. The flood fill algorithm implemented here is similar to the one we utilized to determine blocked regions in porous materials.[12] After identfiying the distinct number of accessible regions at $x = 0$, each of these sections are analyzed separately in subsequent analysis. To analyze the entire channel, we compute the sum of Boltzmann weights along the y,z plane slice at a given x value for all grid points that are connected to the initial accessible region at $x = 0$. The algorithm continues from $x = 0$ to $x = l_x$, where l_x is the unit cell size along the x-direction. If at any point, we encounter a dead-end (i.e., y,z plane where sum of Boltzmann weights is zero) we conclude that the channel does not exist along this region and proceed to the next possible candidate either along the same x direction or along y or z directions. Upon successful traversal to the end of the unit cell, the sum of Boltzmann weights for each value of x can be utilized to identfiy the peak/trough of the free energy profiles for that specific channel along the x-direction. The entire free-energy profile is utilized to compute the diffusion coefficient given that there can be multiple lattice sites along the same channel. The diffusion coefficient value of an individual channel can be obtained from the TST[33,34] taking into account multiple hop-rates generated from the analysis assuming a random walk along the lattice sites. The total diffusion coefficient value along a given direction (e.g D_x) consists of linear combination of the channel diffusion coefficients weighted by its local Henry coefficient values.

dx.doi.org/10.1021/ja400267g | J. Am. Chem. Soc. 2013, 135, 7545−7552

Finally, the total self-diffusion coefficient is calculated as $D_S = {}^1/_3 (D_x + D_y + D_z)$.

Throughout this work, the effects of adsorbate concentration on the diffusion behavior were neglected in order to allow for extremely fast diffusion characterization. The sensitivity of the diffusion coefficients for different loading values will vary based on the structure topology, but is not expected to impact these results significantly. In fact, the assumption of constant diffusion coefficient is commonly used in applications.[32]

Grand Canonical Monte Carlo Simulations. GCMC simulations were utilized to obtain the gas uptake value as a function of fugacity. In GCMC, the chemical potential, volume, and temperature are kept constant throughout the simulation and random insertion, deletion, and translation moves were used to propagate the MC system from one cycle to the next. We have utilized various efficient techniques such as density biased sampling, energy grid usage, and parallelization of energy calculations to reduce the average overall wall time of a single GCMC simulation to under a minute.[35] The number of equilibration cycles and production cycles were set respectively at 250 000 and 100 000. The mixture isotherms were obtained from the computed pure isotherm data using the IAST, which has been demonstrated to be generally applicable to make good predictions about mixture behaviors for various porous materials.[28] It is important, however, to note that some particular cases may need some variant theories of IAST,[36] which is regarded to be out of the scope for this current work.

■ ASSOCIATED CONTENT

Supporting Information

Illustration of a CH_4/CO_2 membrane separation process, detailed derivation of an ideal membrane system for binary separation application, and a figure that relates CO_2 Henry coefficient and self-diffusion coefficient for a large database of zeolite materials. This material is available free of charge via the Internet at http://pubs.acs.org.

■ AUTHOR INFORMATION

Corresponding Author

jihankim@lbl.gov

Notes

The authors declare no competing financial interest.

■ ACKNOWLEDGMENTS

J.K. was supported by the Assistant Secretary for Fossil Energy of the U.S. Department of Energy under Contract No. DE-AC02-05CH11231. M.A. was supported by the Advanced Research Projects Agency–Energy (ARPA-E), U.S. Department of Energy. L.-C.L. was supported by the Deutsche Forschungsgemeinschaft (DFG, priority program SPP 1570). B.S. was supported as part of the Center for Gas Separations Relevant to Clean Energy Technologies, an Energy Frontier Research Center funded by the U.S. Department of Energy, Office of Science, Office of Basic Energy Sciences, under Award No. DE-SC0001015.

■ REFERENCES

(1) Metz, B.; Davidson, O.; deConinck, H.; Loos, M.; Meyer, L. *IPCC Special Report on Carbon Dioxide Capture and Storage*; Intergovernmental Panel on Climate Change: Geneva, Switzerland, 2005; http://www.ipcc.ch.

(2) Chu, S. *Science* **2009**, *325*, 1599.

(3) Lin, L.-C.; Berger, A.; Martin, R. L.; Kim, J.; Swisher, J. A.; Jariwala, K.; Rycroft, C. H.; Bhown, A.; Deem, M. W.; Haranczyk, M.; Smit, B. *Nat. Mater.* **2012**, *11*, 633–641.

(4) Merkel, T. C.; Lin, H.; Wei, X.; Baker, R. *J. Membr. Sci.* **2010**, *359*, 126–139.

(5) Ferey, G. *Chem. Soc. Rev.* **2008**, *37*, 191–214.

(6) Yaghi, O. M.; O'Keeffe, M.; Ockwig, N.; Hee, C.; Eddaoudi, M.; Kim, J. *Nature* **2003**, *423*, 708–714.

(7) D'Alessandro, D. M.; Smit, B.; Long, J. R. *Angew. Chem., Int. Ed.* **2010**, *49*, 6058–6082.

(8) Sumida, K.; Rogow, D. L.; Mason, J. A.; McDonald, T. M.; Bloch, E. D.; Herm, Z. R.; Bae, T.-H.; Long, J. R. *Chem. Rev.* **2012**, *2*, 724–781.

(9) Krishna, R.; van Baten, J. M. *Phys. Chem. Chem. Phys.* **2011**, *13*, 10593–10616.

(10) Krishna, R.; Long, J. R. *J. Phys. Chem. C* **2011**, *115*, 12941–12950.

(11) Wilmer, C. E.; Leaf, M.; Lee, C. Y.; Farha, O. K.; Hauser, B. G.; Hupp, J. T.; Snurr, R. Q. *Nat. Chem.* **2012**, *4*, 83–89.

(12) Kim, J.; Martin, R. L.; Ruebel, O.; Haranczyk, M.; Smit, B. *J. Chem. Theory Comput.* **2012**, *8*, 1684–1693.

(13) Kim, J.; Lin, L.-C.; Swisher, J. A.; Haranczyk, M.; Smit, B. *J. Am. Chem. Soc.* **2012**, *134*, 18940–18943.

(14) Wilmer, C. E.; Farha, O. K.; Bae, Y. S.; Hupp, J. T.; Snurr, R. Q. *Energy Environ. Sci.* **2012**, *5*, 9849–9856.

(15) Kusakabe, K.; Kuroda, T.; Morooka, S. *J. Membr. Sci.* **1998**, *148*, 13–23.

(16) Haldoupis, E.; Nair, S.; Sholl, D. *Phys. Chem. Chem. Phys.* **2011**, *13*, 5053–5060.

(17) First, E.; Chrysanthos, E.; Gounaris, J.; Floudas, A. *Phys. Chem. Chem. Phys.* **2011**, *13*, 17339–17358.

(18) Martin, R.; Smit, B.; Haranczyk, M. *J. Chem. Info. Modelling* **2012**, *52*, 308–318.

(19) Dubbeldam, D.; Beerdsen, E.; Vlugt, T.; Smit, B. *J. Chem. Phys.* **2005**, *122*, 224712.

(20) Abouelnasr, M.; Smit, B. *Phys. Chem. Chem. Phys.* **2012**, *14*, 11600–11609.

(21) (a) Baerlocher, C.; Meier, W. M.; Olson, D. H. *Atlas of Zeolite Framework Types*, 7th ed.; Elsevier: Amsterdam, 2007. (b) http://www.iza-online.org/ (accessed Jan 1, 2010).

(22) Pophale, R.; Deem, M. W.; Cheeseman, P. A. *Phys. Chem. Chem. Phys.* **2011**, *13*, 12407–12412.

(23) Wilems, T. F.; Rycroft, C. H.; Kazi, M.; Meza, J. C.; Haranczyk, M. *Microporous Mesoporpous Mater.* **2012**, *149*, 134–141.

(24) Haldoupis, E.; Nair, S.; Sholl, D. S. *J. Am. Chem. Soc.* **2010**, *132*, 7528–7539.

(25) Tsapatsis, M. *Science* **2011**, *334*, 767–768.

(26) Snyder, M. A.; Tsapatsis, M. *Angew. Chem., Int. Ed.* **2007**, *46*, 7560–7573.

(27) Robeson, L. M. *J. Membr. Sci.* **1991**, *62*, 165–185.

(28) Myers, A. L.; Prausnitz, J. M. *AICHE* **1965**, *11*, 121–130.

(29) Freeman, B. D. *Macromolecules* **1999**, *32*, 375–380.

(30) Krishna, R.; van Baten, J. M. *J. Membr. Sci.* **2010**, *360*, 323–333.

(31) Garcia-Perez, E.; Parra, J. B.; Ania, C. O.; Garcia-Sanchez, A.; van Baten, J. M.; Krishna, R.; Dubbeldam, D.; Calero, S. *Adsorption* **2007**, *13*, 469–476.

(32) Smit, B.; Maesen, T. *Chem. Rev.* **2008**, *108*, 4125–4184.

(33) Ruthven, D. M.; Derrah, R. I. *J. Chem. Soc., Faraday Trans.* **1972**, *68*, 2332–2343.

(34) June, R. L.; Bell, A. T.; Theodorou, D. N. *J. Phys. Chem.* **1991**, *95*, 8866–8878.

(35) Kim, J.; Smit, B. *J. Chem. Theory Comput.* **2012**, *8*, 2336–2343.

(36) Swisher, J. A.; Lin, L.-C.; Kim, J.; Smit, B. *AICHE J.* **2013**, DOI: 10.1002/aic.14058.